Acta Crystallographica Section B
Structural Science
ISSN 0108-7681

Structural characterization of the $n = 5$ layered perovskite neodymium titanate using high-resolution transmission electron microscopy and image reconstruction

Maria Sayagués,[a] Katherine Titmuss,[b] Rudiger Meyer,[b] Angus Kirkland,[b]* Jeremy Sloan,[c] John Hutchison[b] and Richard Tilley[d]

[a]Instituto de Ciencia de Materiales de Sevilla CSIC c/ Americo Vespucio, s/n 41092, Sevilla, Spain, [b]Department of Materials, University of Oxford, Parks Road, Oxford OX1 3PH, England, [c]Inorganic Chemistry Laboratory, University of Oxford, South Parks Road, Oxford OX1 3QR, England, and [d]Division of Materials and Minerals, School of Engineering, University of Wales, Cardiff CF2 1YH, Wales

Correspondence e-mail: angus.kirkland@materials.ox.ac.uk

Received 28 January 2003
Accepted 7 May 2003

The structure of $Nd_5Ti_5O_{17}$ has been refined from a reconstruction of the specimen exit-plane wave restored from a series of incrementally defocused high-resolution transmission electron microscope (HRTEM) images. The phase of the exit-plane wave shows contrast attributable to the oxygen anion sublattice and coupled with simulations provides confirmation of the composition of the cation sites as a function of sample thickness. The enhanced resolution in the exit-plane wave additionally allows a direct measurement of the 'skewing' of the perovskite slabs.

1. Introduction

Perovskites and related structures are of great interest owing to their technologically important physical properties, including ferromagnetism, metallic behaviour at low temperature (Williams *et al.*, 1991) and dielectric properties (Levin *et al.*, 1998), which arise from the structural distortions of the 'ideal' or basic perovskite structure.

The $Nd_5Ti_5O_{17}$ phase belongs to the series $A_nB_nO_{3n+2}$, whose members are oxygen-rich perovskites (Lichtenberg *et al.*, 2001). Within this series the excess anions are accommodated by slicing the cubic perovskite structure parallel to its [110] axis giving perovskite layers nBO_6 units thick. Between these $(A_{n-1}B_nO_{3n+2})_\infty$ perovskite slabs are layers of A cations coordinated by oxygen anions in a rocksalt-type structure (Fig. 1; Sloan & Tilley, 1994; Tilley, 1980). The A cations are generally alkaline earth or lanthanide metals and the B cations are usually titanium or niobium (Lichtenberg *et al.*, 2001).

Typical distortions observed in these systems include tilting of the BO_6 octahedra and displacement of either or both the A and B cations. The former has been widely investigated, to the extent that various systems for categorizing the tilts present in a perovskite have been derived (Glazer, 1975; Thomas, 1996). $La_5Ti_5O_{17}$, which is structurally similar to $Nd_5Ti_5O_{17}$ (Sloan & Tilley, 1994), exhibits a pronounced skewing of the constituent perovskite slabs when observed in the [100] projection (Williams *et al.*, 1991), which hence might also be expected in the neodymium member of the same series.

This paper presents a structural refinement of $Nd_5Ti_5O_{17}$ using a modified through-focal-series high-resolution trans-

Table 1
Unit-cell parameters for $Nd_5Ti_5O_{17}$ measured from electron diffraction patterns.

a (Å)	b (Å)	c (Å)	β (°)
7.8	5.7	31.6	97.71

mission electron microscopy (HRTEM) image reconstruction. This technique reconstructs the *complex* electron wavefunction at the exit plane of the specimen at a resolution approaching the information limit of the microscope (Kirkland *et al.*, 1995, 1997) and deconvolves the effects of the objective lens aberrations. The underlying theory for this reconstruction process is well established (Meyer *et al.*, 2002; Saxton, 1988) and examples of successful reconstructions from defocus series providing information at close to the stated limit have been reported (Kirkland *et al.*, 1995, 1997; Meyer *et al.*, 2002; Saxton, 1988; Coene *et al.*, 1992). Recovering the unaberrated wavefunction in both modulus and phase provides information from lighter scattering elements and improves the directly interpretable resolution and signal-to-noise ratio compared with a single conventional HRTEM image. In the case of $Nd_5Ti_5O_{17}$, the additional information recovered from the oxygen sublattice has allowed the detailed structural characterization described in this article.

2. Experimental

In this study, $Nd_5Ti_5O_{17}$ was synthesized by arc melting from the starting materials Nd_2O_3, TiO_2 and Johnson Matthey 'Specpure' Ti sponge in the appropriate composition along the respective $NdTiO_3$–$Nd_4Ti_4O_{14}$ phase line as described previously (Sloan & Tilley, 1994; Connolly *et al.*, 1996). The arc-melted beads were initially crushed in a percussion mortar and then finely ground in an agate mortar and pestle under acetone.

TEM specimens were prepared from suspensions of each preparation, pipetted onto lacey carbon-coated copper grids (Agar, 300 mesh). Electron diffraction (ED) patterns were obtained from the [010] and [100] zone axes using a Jeol JEM 4000EX(II) electron microscope operated at 400 kV. Energy-dispersive X-ray microanalysis (EDX) spectra were collected using a Jeol JEM 2010 electron microscope equipped with a Link Pentafet/ISIS EDX system using a 5 nm diameter probe. The Nd:Ti ratio was determined by comparison with a phase-pure sample of $NdTiO_3$ as a reference standard. Focal series of high-resolution images were obtained from both the [010] and [100] orientations using a Jeol JEM 3000F field-emission-gun transmission electron microscope (FEGTEM; C_s = 0.57 mm at 300 kV; Kirkland *et al.*, 1999). Images were recorded digitally using a 1024 × 1024 pixel CCD camera mounted axially (Meyer *et al.*, 2000) using a primary microscope magnification of 400 000×. The microscope was manually aligned to the coma-free axis and the twofold astigmatism corrected using on-line diffractograms from the amorphous carbon support film. For each orientation a series of 30 images was recorded of a thin crystal edge beginning under focus with a nominal focal increment of 10 nm towards over focus between images. A final image at the starting defocus was also recorded in order to assess the focal drift. The acquisition of these images was fully automated using scripts running under *Gatan Digital Micrograph Software*. A series of library programs in the *Semper* (Saxton *et al.*, 1979) image-processing package were used to determine the residual objective-lens aberrations and to reconstruct the wavefunction at the exit plane of the specimen using techniques described in full elsewhere (Kirkland *et al.*, 1995, 1997; Meyer *et al.*, 2002; Saxton, 1988).

Simulations were calculated using the standard multislice algorithm (Cowley & Moodie, 1957; Goodman & Moodie, 1974) with simulated exit-plane wavefunctions (corresponding to those recovered experimentally) generated by Fourier-space multiplication of the calculated exit-plane wave with the experimental transfer function effective in the reconstruction.

3. Results and discussion

Lattice parameters measured from ED patterns obtained from the [010] and [100] zone axes of $Nd_5Ti_5O_{17}$ (Table 1, Fig. 2) were similar to those reported for $La_5Ti_5O_{17}$ (Williams *et al.*, 1991). In the [$h0l$] zone systematic absences occur at $h0l$, $l = 2n + 1$ consistent with a c glide (Fig. 2*a*). However, in the $0kl$ zone reflections with $00l$, $l = 2n + 1$ and $0k0$, $k = 2n + 1$ are not absent as expected but are very weakly present; this is attributed to dynamical diffraction from this thicker crystal. If the $00l$, $l = 2n + 1$ are regarded as absent, then this is compatible with a c glide and similarly if $0k0$, $k = 2n + 1$ are also regarded as absent this is consistent with a 2_1 screw axis. Accordingly, we have assigned $Nd_5Ti_5O_{17}$ to the space group $P2_1/c$ in contrast to the assignment of $La_5Ti_5O_{17}$ to Pc (Williams *et al.*, 1991) or to the assignment of the compound $Nd_4Ti_4O_{14}$ to $P2_1$ (Sheunemann & Müller-Buschbaum, 1995). Previous reports of this structure (Sloan & Tilley, 1994) suggest an a parameter of half our stated value. Williams *et al.* (1991) also halved the a value measured from ED patterns as they found no real-space evidence explaining the doubled

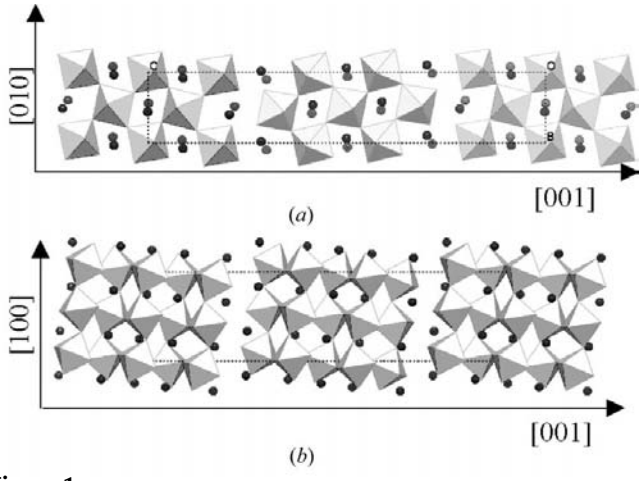

Figure 1
The structure of $Nd_5Ti_5O_{17}$ in (*a*) the [100] projection and (*b*) the [010] projection.

value in reciprocal space. However, the improved resolution provided by restoring the exit-plane wavefunction reveals the structural cause of this doubling, which is discussed in §3.1.

For detailed structural interpretation, the phase and modulus of the exit wavefunctions were restored from focal series obtained from both [010] and [100] projections. The restored phase and the modulus for both projections (Fig. 3) contain largely complementary information; the modulus shows high-resolution information about the cation lattice which is relatively insensitive to specimen thickness, contamination layers and the support film, whereas the phase provides information about both the cation lattice and weakly scattering elements such as oxygen (Saxton, 1988; Kirkland *et al.*, 1997). The modulus can therefore be used to obtain accurate cation coordinates from the location of the peaks which are restored in positive contrast and to higher resolution than in a conventional HRTEM image. The phase also shows reversed contrast peaks at corresponding sites, but in addition provides limited direct information about the anion sublattice from weak subsidiary peaks located between the cation sites.

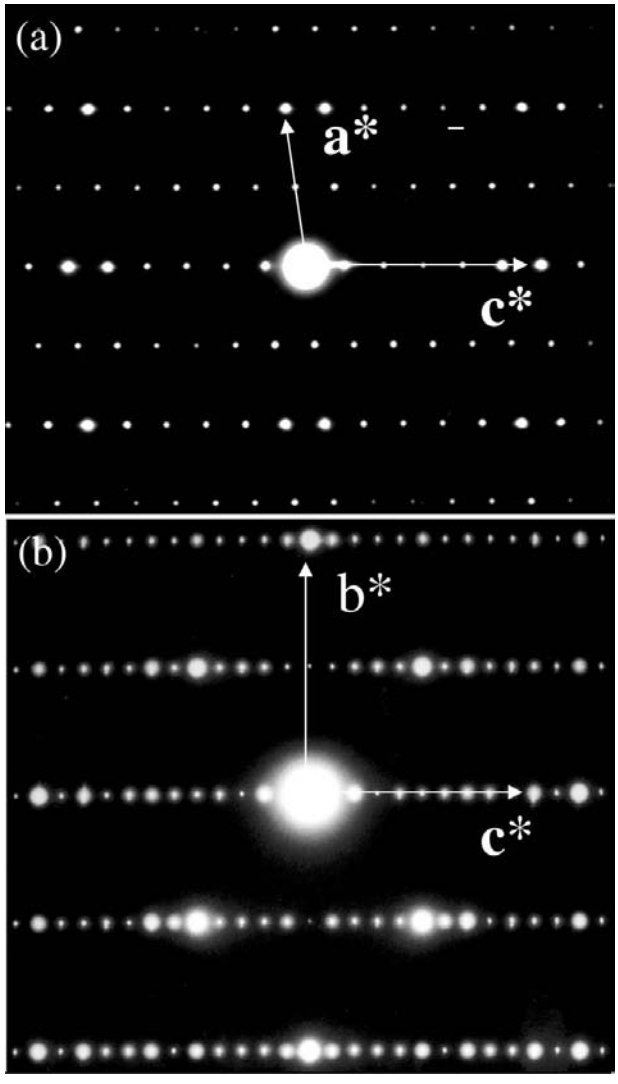

Figure 2
Selected-area electron diffraction (ED) patterns recorded for two different crystals of $Nd_5Ti_5O_{17}$. (*a*) Parallel to [010] with all *l*-odd reflections absent. (*b*) Parallel to [100] with 00*l*, *l*-odd reflections and 0*k*0, *k*-odd reflections only very weakly present, as discussed in the text.

3.1. Analysis of the exit wavefunction modulus

The structure of $Nd_5Ti_5O_{17}$ has previously been reported as identical to $La_5Ti_5O_{17}$ (Sloan & Tilley, 1994). The enhanced resolution of the modulus compared with the conventional axial image (Fig. 3) allows a more accurate direct measurement of the cation coordinates so that a comparison with those reported for $La_5Ti_5O_{17}$ (Williams *et al.*, 1991) can now be made.

Cation coordinates were extracted from the [100] and the [010] projections by taking 256 × 256 pixel regions from the edge of each crystal and lattice averaging each within these. This further enhanced the peaks at each atom site by reducing noise, but over areas sufficiently small to retain any local lattice distortions. The *Semper* command *SPC* was then used to overlay each lattice average with a contour map and the cation positions were recorded and the variance in their positions was calculated.

Fig. 4 shows a plot of the cation coordinates measured from the modulus in both [100] and [010] projections with an estimate of the error based on the standard deviation determined

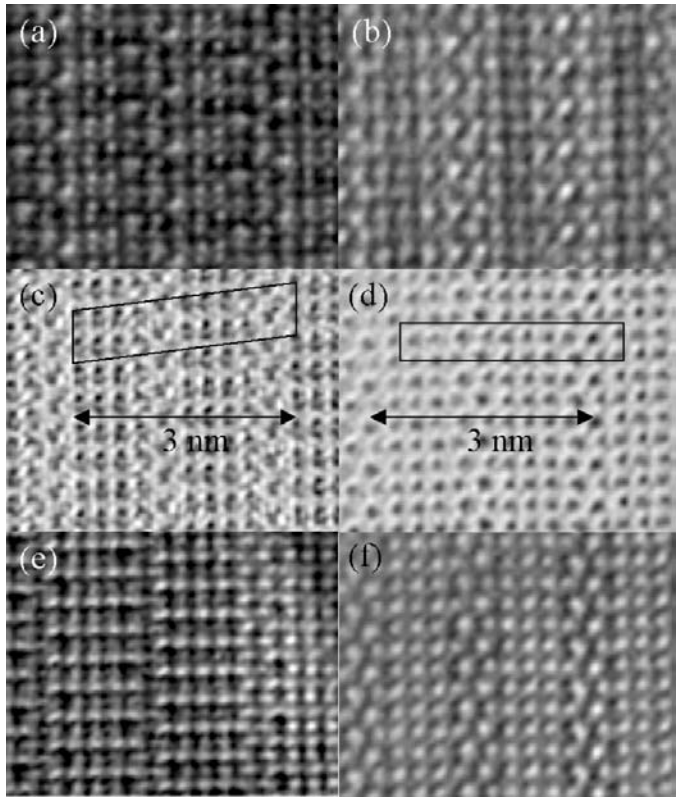

Figure 3
Unprocessed axial images in (*a*) [010] and (*b*) [100] projections recorded at approximately the Scherzer defocus. Restored modulus of the exit-plane wavefunction in (*c*) [010] and (*d*) [100] projections. Restored phase of the exit-plane wavefunction in (*e*) [010] and (*f*) [100] projections. Unit cells are outlined in (*c*) and (*d*).

from the values measured from the different averaged areas of the crystal.

Our data suggest that an improved model for $Nd_5Ti_5O_{17}$ could be constructed based on the bulk perovskite $NdTiO_3$ (Amow & Greedan, 1996), which differs from the archetypal cubic perovskite by a tilting of its octahedra. A preliminary model was therefore built by dividing this perovskite bulk into slabs, five BO_6 octahedra in width. Adjacent slabs were then shifted with respect to one another along the *a* axis by $a/4$ and the extra two oxygen anions per unit cell required to maintain stoichiometry were accommodated at the interface between the two slabs.

Comparison of simulations calculated from this model with the experimental restored modulus showed that the central section in the perovskite slabs of $Nd_5Ti_5O_{17}$ matched very well. However, to produce a good overall match two further modifications to the cation lattice were necessary. The first alteration was to shift the outer neodymium cations further away from the slab center by a displacement parallel to the *c* axis measured from the experimental restored modulus. In Fig. 5(*b*) (where for clarity the oxygen anions are omitted and only one of the two slabs that compose a unit cell is shown) this is marked as displacements, δ_1 and δ_2, from the position expected for the bulk perovskite $NdTiO_3$. The displacement alternates between two values and in the expanded section of the modulus shown in Fig. 5(*a*), this is clearly visible where the interface neodymium cations (circled in Fig. 5*a*) move alternately in opposite directions. This cation displacement is the origin of the doubling of the *a* repeat and the perovskite slabs are stacked in a regular way such that the geometry is the same at each interface. This measurement of the cation displacements is based on data obtained from the thin crystal edge, however, it is entirely consistent with electron diffraction patterns recorded from larger areas of the bulk crystal.

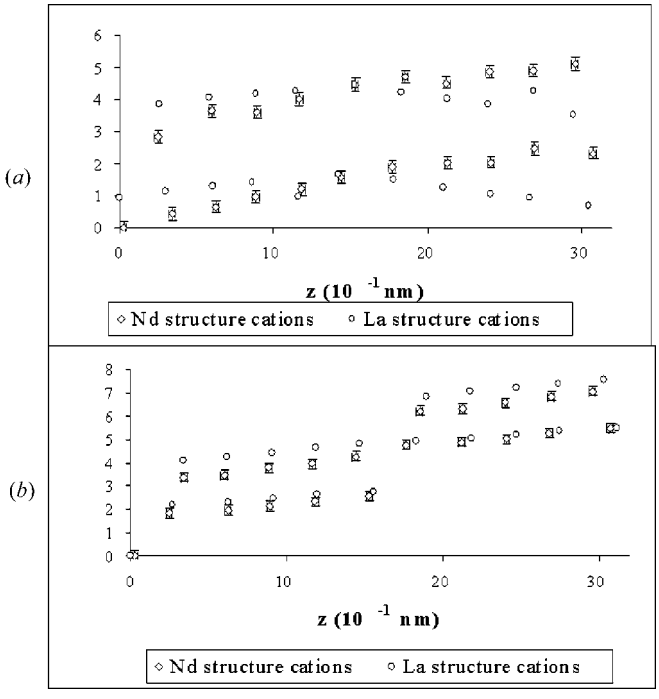

Figure 4
Cation coordinates measured for $Nd_5Ti_5O_{17}$ from the restored modulus for (*a*) [010] and (*b*) [100] projections. Included for comparison are the corresponding $La_5Ti_5O_{17}$ coordinates.

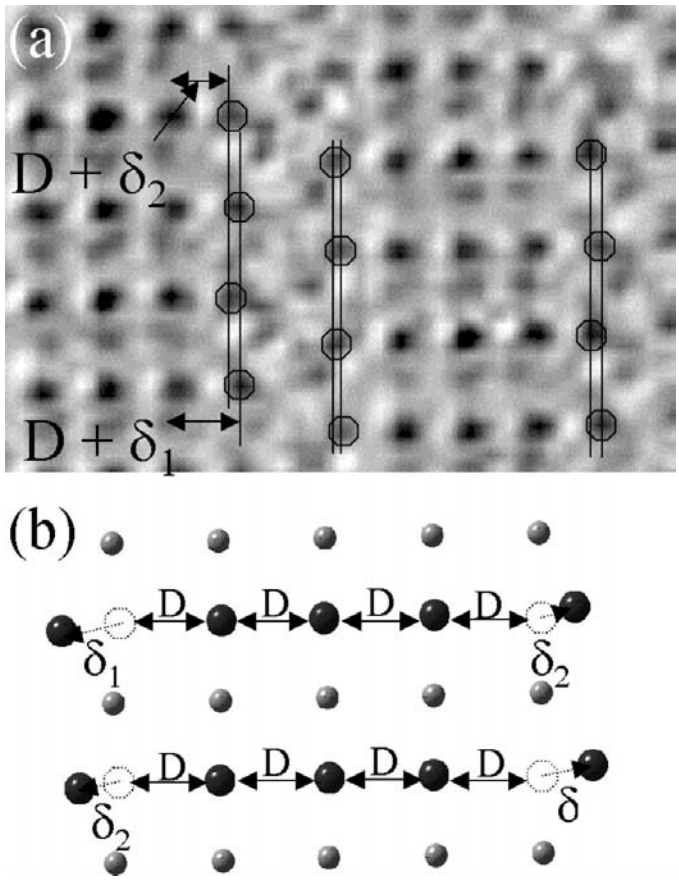

Figure 5
(*a*) Enlargement of the experimentally restored modulus showing the displacements of the neodymium cations at the slab interface in $Nd_5Ti_5O_{17}$. (*b*) Illustration of the shift in neodymium cation positions at the slab interface compared with their position in $NdTiO_3$.

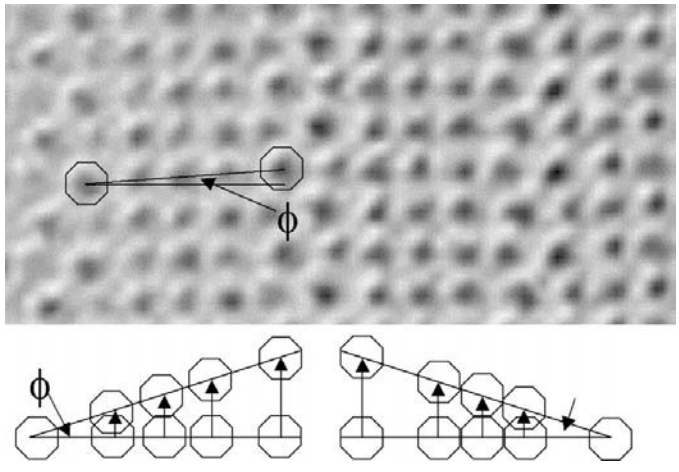

Figure 6
Restored exit-plane modulus in the [010] projection together with a schematic illustration of the effect on coordinates in the *b* direction of the skew of the perovskite slabs.

The second modification required is to allow for a 'skew' of the slabs which is clearly observed along [100] and which has also been observed in $La_5Ti_5O_{17}$, where it was described as a 'canting' of the slabs (Williams *et al.*, 1991). The skew is defined by an angle ϕ to the original axis and the new coordinates are produced from the dot product of the original coordinates with the skew vector, with neighbouring slabs skewed by φ acting alternately clockwise and anticlockwise. The effect of this skew is to shift the coordinates along the *b* axis by increasing amounts as *c* increases (Fig. 6). This skewing of the perovskite slabs is a reflection of the perovskite structure's flexibility in accommodating a wide range of cation sizes through various distortion mechanisms. In the context of other more common distortions, it is necessary to consider the basic cubic perovskite structure and the reasons for its distortion with changing cation sizes. In the basic perovskite structure, the *A* cations are accommodated in cuboctahedral sites, coordinated by 12 O^{2-} ions and for an ideal structure ($SrTiO_3$), the *A* cation is centrally positioned within this interstice (Fig. 7). Where the cations are too small to occupy a 12 coordinated site (as with $NdTiO_3$ owing to the 'lanthanide contraction'), the structure distorts in order to reduce the *A* cation coordination. One commonly observed distortion

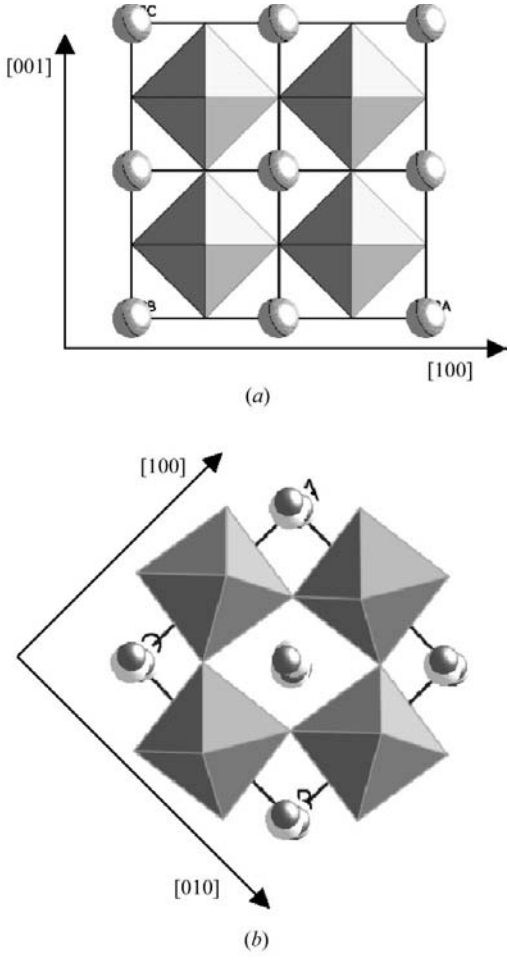

Figure 7
(*a*) The cubic perovskite $SrTiO_3$. (*b*) The perovskite $NdTiO_3$ showing the octahedral tilts referred to in the text.

Table 2
Skew of the perovskite slabs in $Nd_5Ti_5O_{17}$ measured from the restored modulus in the [100] projection.

	Skew in Nd rows	Skew in Ti rows
Skew, φ (°)	3.0	1.8
Standard deviation in the measurements	0.4	0.6

which achieves this is a tilt of the BO_6 octahedra around one or more axes, as observed for the LaMO_3 family (Fig. 7) and in the related Ruddlesden–Popper layered perovskites of the general formula $A_nB_nX_{3n+1}$ (Hamada *et al.*, 1997). This skewing can be considered as an additional mechanism available to reduce the coordination of the *A* cation sites by distorting the cation positions away from the basic cubic perovskite geometry.

For $Nd_5Ti_5O_{17}$ the angle φ was measured in *Semper* (Saxton *et al.*, 1979) by extracting a perovskite slab from the restored modulus and calculating its mirror image. This mirror image was then skewed along the *b* direction by extracting it with a range of base vectors and measuring the correlation coefficient between the extracted and the original images. Using this method it has been possible to measure φ to high precision and Table 2 shows that φ for the $Nd_5Ti_5O_{17}$ slabs is larger than the 1° previously measured for $La_5Ti_5O_{17}$ (Williams *et al.*, 1991).

Table 3 lists cation radii for Nd^{III} and La^{III} and also a range of alkali earth metals to give an indication of more typical perovskite cation sizes. The Nd^{III} cation is 0.01 nm smaller in radius than La^{III} and so the increased distortion for Nd^{III} compared with La^{III} is in agreement with other perovskite studies (Hamada *et al.*, 1997; Elcombe *et al.*, 1991; Teneze *et al.*, 2000) that show greater distortion for smaller *A* cations.

3.2. Analysis of the exit wavefunction phase

The most striking information gained from the phase, which is absent in the modulus, is additional weak contrast between the cation site positions. The model of the [010] projection (Fig. 1) shows slabs, five octahedra thick, composed of alternate rows of neodymium and titanium atoms with the titanium bridged by linking oxygen. Correspondingly, the phase restored from the [010] projection (Fig. 3) shows rows of five isolated atom sites alternating with rows of five weaker sites with additional weak contrast between the cation sites in these rows. Multislice simulations for the [010] projection for a fully oxygenated structure and a deoxygenated fraction (Fig. 8) show an absence of contrast between the Ti atoms for the hypothetical cation-only model, which strongly suggests that the contrast seen in the phase image between the Ti atoms is due to the oxygen anion sublattice.

This observation of the oxygen contrast in the restored phase of the [010] projection has also allowed the neodymium and titanium sites to be easily distinguished. For a weak (complex) object the observed contrast in the restored phase is related to the atomic number of the atom sites in projection. In the thin-specimen regions at the edge of the sample, the relative contrast is as predicted by this approximation with

Table 3
Ionic radii (Å) of a selection of alkaline earth and lanthanide cations (Lide, 1999).

Radii are given for a 12-coordinated cation unless this does not exist, in which case the coordination number is given in parentheses. Both Ti^{IV} and Ti^{III} are given as Ti has a formal oxidation state of 3.75 in $La_5Ti_5O_{17}$.

Ion	Ionic radius	Ion	Ionic radius
Ca^{II}	1.34	La^{III}	1.36
Sr^{II}	1.44	Ce^{III}	1.34
Ba^{II}	1.61	Pr^{III} (8)	1.13
Ti^{IV} (8)	0.61	Nd^{III}	1.27
Ti^{III} (8)	0.67		

neodymium appearing brighter than titanium. However, as the sample thickness increases, the relative contrast of these sites reverses such that titanium appears brighter than neodymium (Fig. 9*a*).

Investigation of the variation in the relative intensities of these sites in the restored phase with thickness was carried out using multislice calculations for a range of thicknesses for both the [100] and the [010] orientations. The results are plotted (Figs. 9*b* and *c*) as differences between the phase at adjacent neodymium and titanium sites in the center of the perovskite slabs. The crossover points therefore indicate those thicknesses at which the phase difference is zero.[1] The simulated phase difference in the [100] projection as a function of thickness indicates that for a range of thicknesses, *R* (Fig. 9*b*), the phase difference between the neodymium and titanium sites is nearly zero under which conditions the neodymium and titanium are indistinguishable, as observed experimentally (Fig. 3*f*). However, in the simulated phase difference (Fig. 9*c*) for the [010] projection, the contrast reverses sharply as the crystal thickness increases, suggesting that the region of the contrast reversal in the experimental restored phase (Fig. 9*a*) corresponds to the thickness at which the first reversal, marked F, in Fig. 9(*c*) occurs.

Overall, therefore, this detailed analysis of individual site contrast in the phase of the exit-plane wavefunction allows the neodymium and titanium cation sites to be distinguished and provides a potentially sensitive measure of thickness for very thin crystals.

4. Conclusions

The improved resolution and additional data offered by reconstruction of the specimen exit-plane wavefunction has allowed an improved structural determination of $Nd_5Ti_5O_{17}$ which accounts for the doubled *a* repeat measured from ED patterns by a shifting of the *A* cations at the slab interfaces. A similar shift of the *A* cations may also be responsible for the doubling of the *a* repeat seen in ED patterns of the closely related $La_5Ti_5O_{17}$ structure. The skewing of the perovskite slabs has also been directly measured and shown to be larger than that for $La_5Ti_5O_{17}$, most likely resulting from the decreasing radius of the *A* cation.

The restored phase of the [010] orientation showed weak contrast due to the oxygen sublattice which enabled the neodymium and titanium sites to be distinguished and indicated a contrast reversal with thickness for the neodymium and titanium sites. This contrast reversal provides an accurate method for estimating the crystal thickness, even for very thin specimens.

[1] Note that in the [100] projection, the titanium site is in fact a mixed titanium and oxygen column and in the [010] projection, the neodymium site is a mixed neodymium and oxygen column.

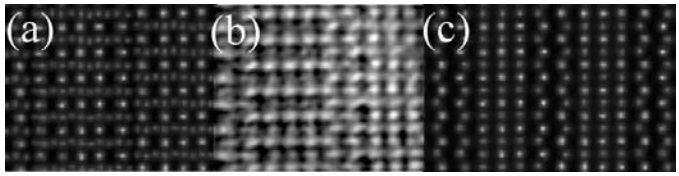

Figure 8
(*a*) Multislice simulation of $Nd_5Ti_5O_{17}$. (*b*) Phase of the experimental restored exit-plane wavefunction in the [010] projection. (*c*) Multislice simulation of a hypothetical model based on the cation lattice of $Nd_5Ti_5O_{17}$ with all oxygen anions absent.

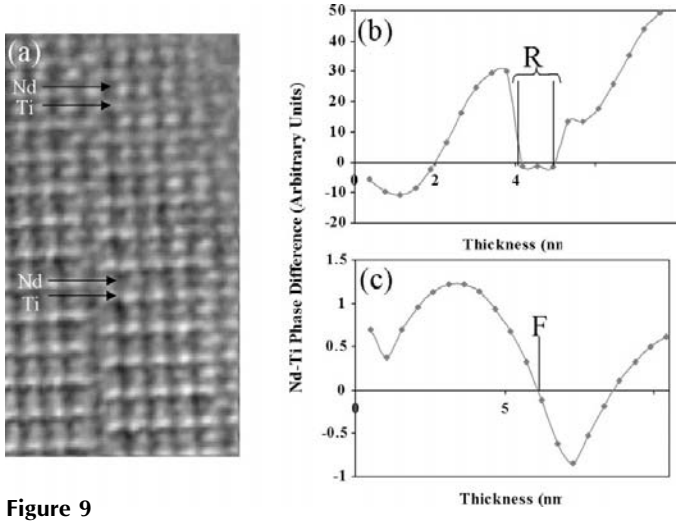

Figure 9
(*a*) Reversal in the relative intensity at the neodymium and titanium sites in the restored phase as a function of crystal thickness for the [010] projection. Simulated phase difference between Nd and Ti for (*b*) the [100] and (*c*) the [010] projections as a function of thickness.

The authors are grateful to Dr D. J. Watkin for his assistance with the assignment of space groups. MJS is grateful to ROPA grant GR/K36492 for financial support. JS is indebted to the G. H. Latham Foundation (University of Wales) and the Royal Society for financial support. AIK acknowledges financial support from the EPSRC (Grant GR/N17577) and the Leverhulme Trust.

References

Amow, G. & Greedan, J. E. (1996). *J. Solid State Chem.* **121**, 443–450.
Coene, W., Janssen, G., Op de Beeck, M. & van Dyck, D. (1992). *Phys. Rev. Lett.* **69**, 3743–3747.

Connolly, E., Sloan, J. & Tilley, R. J. D. (1996). *Solid State Inorg. Chem.* **33**, 360–369.
Cowley, J. M. & Moodie, A. F. (1957). *Acta Cryst.* **10**, 609–619.
Elcombe, M., Kisi, E. H., Hawkins, K., White, T., Goodman, P. & Matheson, S. (1991). *Acta Cryst.* B**47**, 305–314.
Glazer, A. M. (1975). *Acta Cryst.* A**31**, 756–762.
Goodman, P. & Moodie, A. F. (1974). *Acta Cryst.* A**30**, 280–290.
Hamada, N., Sawaka, H., Solovyev, I. & Terakura, K. (1997). *Physica B*, **11**, 237–238.
Kirkland, A., Meyer, R. & Saxton, O. (1999). In *Electron Microscopy and Analysis 1999*, Vol. 161, *Institute of Physics Conference Series*, p. 291. Institute of Physics.
Kirkland, A. I., Saxton, W. O. & Chand, G. (1997). *J. Electron Microsc.* **1**, 11–22.
Kirkland, A. I., Saxton, W. O., Chau, K. L., Tsuno, K. & Kawasaki, M. (1995). *Ultramicroscopy*, **57**, 355–374.
Levin, I., Bendersky, L. A., Vanderah, T. A., Roth, R. S. & Stafsudd, O. (1998). *Mater. Res. Bull.* **33**, 501–517.
Lichtenberg, F., Herrnberger, A., Wiedenmann, K. & Mannhart, J. (2001). *Prog. Solid State Chem.* **29**, 1–70.
Lide, D. (1999). Editor. *CRC Handbook of Chemistry and Physics*. 80th ed. Boca Raton: CRC Press.
Meyer, R., Kirkland, A. I. & Saxton, W. O. (2002). *Ultramicroscopy*, **92**, 89–109.
Meyer, R. R., Kirkland, A. I., Dunin-Borkowski, R. E. & Hutchison, J. L. (2000). *Ultramicroscopy*, **85**, 9–13.
Saxton, W. O. (1988). *Scanning Microsc. Suppl.* **2**, 213–224.
Saxton, W. O., Pitt, T. J. & Horner, M. (1979). *Ultramicroscopy*, **4**, 343–354.
Sheunemann, K. & Müller-Buschbaum, H. (1995). *Inorg. Nucl. Chem.* **37**, 2261–2263.
Sloan, J. & Tilley, R. J. D. (1994). *Eur. J. Solid State Inorg. Chem.* **31**, 673–682.
Teneze, N., Mercurio, D., Trolliard, G. & Frit, B. (2000). *Mater. Res. Bull.* **35**, 1603–1614.
Thomas, N. W. (1996). *Acta Cryst.* B**52**, 16–31.
Tilley, R. (1980). *Chemical Physics of Solids and their Surfaces*, ch. 6, p. 150. London: Royal Society of Chemistry.
Williams, T., Schmalle, H. W., Reller, A., Lichtenberg, F. D. W. & Bednorz, G. (1991). *J. Solid State Chem.* **93**, 534–548.